

Article

Research on Modeling of the Agile Satellite Using a Single Gimbal Magnetically Suspended CMG and the Disturbance Feedforward Compensation for Rotors

Peiling Cui ^{1,2,*} and Ning Yan ^{1,2,3}

- ¹ School of Instrumentation Science and Optoelectronics Engineering, Beihang University, Beijing 100191, China; E-Mail: n_yann@sina.com
- ² Science and Technology on Inertial Laboratory, Beijing 100191, China
- ³ Research and Design Centre, China Academy of Launch Vehicle Technology, Beijing 100076, China
- * Author to whom correspondence should be addressed; E-Mail: peilingcui@buaa.edu.cn; Tel.: +86-10-8233-9273.

Received: 9 May 2012; in revised form: 20 November 2012 / Accepted: 22 November 2012 / Published: 12 December 2012

Abstract: The magnetically suspended Control Moment Gyroscope (CMG) has the advantages of long-life, micro-vibration and being non-lubricating, and is the ideal actuator for agile maneuver satellite attitude control. However, the stability of the rotor in magnetic bearing and the precision of the output torque of a magnetically suspended CMG are affected by the rapid maneuvers of satellites. In this paper, a dynamic model of the agile satellite including a magnetically suspended single gimbal control moment gyroscope is built and the equivalent disturbance torque effected on the rotor is obtained. The feedforward compensation control method is used to depress the disturbance on the rotor. Simulation results are given to show that the rotor displacement is obviously reduced.

Keywords: Control Moment Gyroscope; dynamic modeling; feedforward compensation; magnetic bearing

1. Introduction

With the development of high resolution imaging on Earth, the requirement of satellite agility is increasing. The magnetically suspended Single Gimbal Control Moment Gyroscope (SGCMG) is chosen as the ideal actuator for its large output torque to perform rapid maneuver tasks by using the

magnetic bearing instead of traditional mechanical bearing [1-3]. It has the advantage of high precision, long-life, micro-vibration and being non-lubricating [4]. It can be applied for agile maneuver satellite attitude control. For agile satellites, the slew rate is often at the level of $1\sim10^{\circ}/s$ [5], but when the satellite slews fast or the gimbal rotates rapidly, the rotor displacement will be increased and the precision of output torque will be decreased, even leading to rotor instability, so research on agile satellite attitude control using magnetically suspended SGCMGs is very important.

For the control of magnetic bearing systems, scholars have reported some research results [4–7]. For example, cross feedback control of magnetic bearing systems [6], filtered-X least mean square (FXLMS) algorithm for moving-gimbal effects [4], and the compound control for moving-gimbal effect compensation to increase the response of the gimbal system [7]. The research is all based on a static base, and the influence of rapid satellite maneuvers on the rotor displacement is not analyzed.

For the satellite attitude control based on a Control Moment Gyroscope (CMG), there are some research results [8–14]. Reference [12] gives a model of the CMG mechanism and the CMG output torque in body frame. In Reference [13], aiming at solving the problem of high precision and high stability attitude control of satellites, the influence of magnetically suspended rotor dynamic imbalance and static imbalance on the vibration of the base, and the stability of a magnetically suspended control system are investigated. The disturbance torque on the base resulting from the imbalance vibration is reduced. In Reference [14], a dynamic model of a spacecraft with a magnetically suspended single gimbal control moment gyroscope is given, but the slew rate of the satellite is limited at 10^{-2} rad/s level (approximate 0.5° /s). How to use magnetically suspended SGCMGs for the agile maneuver attitude control of the satellite is not mentioned.

In this paper, the dynamic model of the agile satellite including a magnetically suspended single gimbal control moment gyroscope is built and the equivalent disturbance torque effected on the rotor is obtained. The feedforward compensation control method is used to depress the disturbance on the rotor. Simulation results are given to show that the rotor displacement is obviously decreased.

2. The Satellite Attitude Dynamic Model Including a Magnetically Suspended SGCMGs

Different from the mechanical CMG, a magnetically suspended rotor is used in a magnetically suspended CMG. The translational position of the rotor relative to the magnetic bearing can be controlled actively. Besides the high-speed rotation degree, the magnetically suspended CMG has five more degrees of freedom than the mechanical CMG, and thus the modeling process is complex. Firstly, the coordinate frames are needed to be defined. In the following, n = 1, 2, 3, 4 denotes the *n*-th CMG. Figure 1 gives the relationship between inertial frame system, orbit frame, and satellite body frame.

 F_i : Inertia frame $O_i X_i Y_i Z_i$. The origin is the Earth's core, $O_i X_i$ points to the vernal equinox, while $O_i Z_i$ points to the North Pole.

 F_o : Orbit frame $O_o X_o Y_o Z_o$. The origin is the centre of mass of the satellite, $O_o X_o$ and $O_o Y_o$ represent the roll axis and the pitch axis, respectively, both locating in the orbital plane.

 F_b : Satellite body frame $O_b X_b Y_b Z_b$. The origin is the centre of mass of satellite. $O_b X_b$, $O_b Y_b$ and $O_b Z_b$ are along the principal axes of inertia of the satellite.

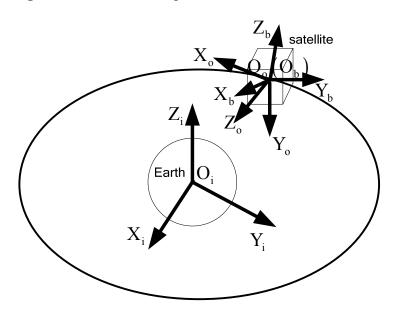


Figure 1. The relationship between the coordinate frames.

 $F_{cmg,n}$: The *n*-th CMG frame $O_{cmg,n}X_{cmg,n}Y_{cmg,n}Z_{cmg,n}$. Fixed with the satellite, but it is determined by configuration. $O_{cmg,n}$ is the rotor centre of mass of the *n*-th magnetically suspended SGCMG, $X_{cmg,n}$ is the gimbal axis, $Y_{cmg,n}$ is the spin direction of the rotor when the gimbal angle is in zero position.

 $F_{g,n}$: The *n*-th gimbal frame $O_{g,n}X_{g,n}Y_{g,n}Z_{g,n}$. Fixed with the gimbal, the frame can rotate with the gimbal. When the gimbal angle is in zero position, the gimbal frame coincides with the CMG frame.

 $F_{f,n}$: The *n*-th magnetic bearing installed frame $O_{f,n}X_{f,n}Y_{f,n}Z_{f,n}$. It is fixed with the gimbal frame.

This frame is obtained by 45° rotation of the gimbal frame and about the Y_{gn} axis.

 $F_{r,n}$: The *n*-th rotor frame $O_{r,n}X_{r,n}Y_{r,n}Z_{r,n}$. It is fixed with the rotor. This frame does not spin with the rotor. $O_{f,n}$ coincides with $O_{r,n}$ when the rotor is not suspended.

 $C_{E}^{F_{2}}$: denotes the coordinate transformation matrix from frame F_{1} to frame F_{2} .

In Section 2.1, the rotor dynamic model of single gimbal magnetically suspended CMG is analyzed. For convenience, the index *n* is omitted. For example, F_g represents the gimbal frame $O_g X_g Y_g Z_g$.

2.1. The Dynamic Model of Magnetically Suspended Rotor

The Euler equation is used to build the magnetically suspended rotor dynamic model. A magnetically suspended SGCMG consists of the rotor and the gimbal. The magnetic force is produced from the unique relation between the rotor and the bearing. In order to perform the satellite attitude control, the direction of angular momentum is changed through magnetic bearing torque by the gimbal rotation, and then the gyroscope torque is generated, and is transmitted to the satellite by the magnetic bearings.

In this paper, the rotor is supposed to be asymmetric, and the dynamic and static vibration induced by the geometry shape are ignored. Only the force induced from the gimbal rotation of the CMG frame relative to the inertial frame is considered. The rotation relationship between CMG frame and the gimbal frame is given in Figure 2.

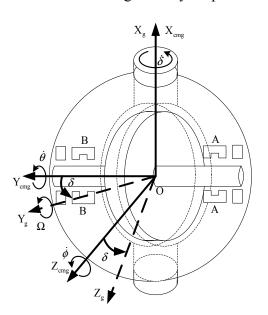
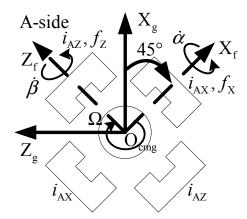


Figure 2. A sketch of the magnetically suspended SGCMG.

As shown in Figure 2, $\dot{\delta}$, $\dot{\theta}$ and $\dot{\phi}$ are the angular velocity of CMG frame relative to gimbal frame. δ is the rotation angle from CMG frame to gimbal frame. $\dot{\delta}$ is the gimbal rate about X_{cmg} axis. Figure 3 denotes the view from A-side about the Y_{cmg} -direction in Figure 2. It shows the relationship between the gimbal frame and the installed magnetic bearing frame. f_X and f_Z denote the radial magnetic bearing force about the X_f -axis and Z_f -axis. f_Y is the axial magnetic bearing force. α and β are the rotation angle of the rotor about the X_f -axis and Z_f -axis, respectively. $\dot{\alpha}$ and $\dot{\beta}$ are the angular velocity about the X_f -axis and Z_f -axis, respectively. Ω is the rotor speed relative to the rotor frame, and it is about Y_f -axis. i_{AX} and i_{AZ} are the magnetic bearing control current about X_f -axis and Z_f -axis of the A-side.

Figure 3. Sketch map of the magnetic bearing installation.



Firstly, only one magnetically suspended SGCMG is analyzed. M^r is the torque acting on the rotor. By using the Euler equation, the magnetically suspended rotor dynamic model in the rotor frame can be obtained:

$$\mathbf{M}^{r} = \dot{\mathbf{H}}^{r} + \boldsymbol{\omega}_{ir}^{r} \times \mathbf{H}^{r}$$
(1)

In Equation (1), ω_{ir}^r denotes the absolute angular velocity in rotor frame. It includes ω_{rf}^f , ω_{icmg}^{cmg} , and ω^g . ω_{rf}^f is the angular velocity of the rotor. It is the magnetic bearing frame relative to the rotor frame, and is shown in the magnetic bearing frame. ω_{icmg}^{cmg} is the angle velocity of CMG frame relative to the inertial frame. ω^g is the gimbal angular velocity:

$$\boldsymbol{\omega}_{ir}^{r} = \mathbf{C}_{f}^{r} \left(\boldsymbol{\omega}_{if}^{f} + \mathbf{C}_{g}^{f} \mathbf{C}_{cmg}^{g} \boldsymbol{\omega}_{ig}^{cmg} \right)$$
(2)

The absolute angle velocity Ω_{ir}^r of the rotor includes the spin rate Ω^r and the rate ω_{ir}^r of the rotor frame:

$$\mathbf{\Omega}_{ir}^{r} = \mathbf{\Omega}^{r} + \mathbf{\omega}_{ir}^{r} = \mathbf{\Omega}^{r} + \mathbf{C}_{f}^{r} \left(\mathbf{\omega}_{rf}^{f} + \mathbf{C}_{g}^{f} \mathbf{C}_{cmg}^{g} \mathbf{\omega}_{ig}^{cmg} \right)$$
(3)

Because α and β are very small, then $\cos \alpha \approx 1$, $\cos \beta \approx 1$, $\sin \alpha \approx \alpha$, $\sin \beta \approx \beta$, $\alpha \beta \approx 0$. Then:

$$\mathbf{C}_{f}^{r} = \begin{bmatrix} \cos\beta & \sin\beta & 0\\ -\sin\beta & \cos\beta & 0\\ 0 & 0 & 1 \end{bmatrix} \begin{bmatrix} 1 & 0 & 0\\ 0 & \cos\alpha & \sin\alpha\\ 0 & -\sin\alpha & \cos\alpha \end{bmatrix} \approx \begin{bmatrix} 1 & \beta & 0\\ -\beta & 1 & \alpha\\ 0 & -\alpha & 1 \end{bmatrix}, \ \mathbf{\omega}_{rf}^{f} = \begin{bmatrix} \dot{\alpha}\\ 0\\ \dot{\beta} \end{bmatrix}$$

$$\mathbf{C}_{g}^{f} = \begin{bmatrix} \cos 45^{\circ} & 0 & -\sin 45^{\circ}\\ 0 & 1 & 0\\ \sin 45^{\circ} & 0 & \cos 45^{\circ} \end{bmatrix}$$

$$(4)$$

By rotating δ about X_{cmg} axis from the CMG frame to the gimbal frame, then:

$$\mathbf{C}_{cmg}^{g} = \begin{bmatrix} 1 & 0 & 0 \\ 0 & \cos \delta & \sin \delta \\ 0 & -\sin \delta & \cos \delta \end{bmatrix}, \ \mathbf{\omega}^{g} = \begin{bmatrix} \dot{\delta} \\ 0 \\ 0 \end{bmatrix}, \ \mathbf{\omega}_{ig}^{cmg} = \mathbf{\omega}_{icmg}^{cmg} + \mathbf{\omega}^{g} = \begin{bmatrix} \dot{\phi} \\ \dot{\theta} \\ \dot{\phi} \end{bmatrix} + \begin{bmatrix} \dot{\delta} \\ 0 \\ 0 \end{bmatrix} = \begin{bmatrix} \hat{\delta} \\ \dot{\theta} \\ \dot{\phi} \end{bmatrix}$$
(5)

where $\hat{\delta}$, $\dot{\theta}$ and $\dot{\phi}$ show the absolute angular velocity of the CMG frame, and the detailed expression will be given in Section 2.2. By substituting the coordinate transformation matrix and the relative angular velocity, then:

$$\boldsymbol{\Omega}_{ir}^{r} = \begin{bmatrix} \frac{\sqrt{2}}{2} \left(\hat{\delta} - \dot{\phi} \cos \delta + \dot{\theta} \sin \delta \right) + \dot{\alpha} + \beta \left(\dot{\theta} \cos \delta + \dot{\phi} \sin \delta \right) \\ \Omega - \frac{\sqrt{2}}{2} \beta \left(\hat{\delta} - \dot{\phi} \cos \delta + \dot{\theta} \sin \delta \right) - \dot{\alpha} \beta + \left(\dot{\theta} \cos \delta + \dot{\phi} \sin \delta \right) - \frac{\sqrt{2}}{2} \alpha \left(\hat{\delta} + \dot{\phi} \cos \delta - \dot{\theta} \sin \delta \right) + \alpha \dot{\beta} \\ \frac{\sqrt{2}}{2} \left(\hat{\delta} + \dot{\phi} \cos \delta - \dot{\theta} \sin \delta \right) + \dot{\beta} - \alpha \left(\dot{\theta} \cos \delta + \dot{\phi} \sin \delta \right) \end{bmatrix}$$
(6)

In Equation (1), \mathbf{H}^{r} is the rotor angular momentum in the rotor frame:

$$\mathbf{H}^{r} = \tilde{\mathbf{I}}_{r} \boldsymbol{\Omega}_{ir}^{r} = \begin{bmatrix} I_{rx} & 0 & 0\\ 0 & I_{ry} & 0\\ 0 & 0 & I_{rz} \end{bmatrix} \boldsymbol{\Omega}_{ir}^{r}$$
(7)

where $\tilde{\mathbf{I}}_r$ denotes the wheel moment of inertia in the spin direction. I_{rx} and I_{ry} are the radial inertia of the magnetically suspended rotor in the x and y direction, respectively. I_{rz} is the axial inertia of the

rotor. The angular momentum variation rate relative to the rotor frame can be obtained from the time derivatives:

$$\dot{\mathbf{H}}^{r} = \begin{bmatrix} I_{rx} \left(\frac{\sqrt{2}}{2} \left(\hat{\delta} - \ddot{\phi} \cos \delta + \dot{\phi} \hat{\delta} \sin \delta + \ddot{\theta} \sin \delta + \dot{\theta} \hat{\delta} \cos \delta \right) \\ + \dot{\beta} \dot{\theta} \cos \delta + \beta \ddot{\theta} \cos \delta - \beta \dot{\theta} \hat{\delta} \sin \delta + \beta \dot{\phi} \sin \delta + \beta \ddot{\phi} \sin \delta + \beta \dot{\phi} \hat{\delta} \cos \delta + \ddot{\alpha} \dot{\theta} \\ I_{ry} \left(\frac{\sqrt{2}}{2} \left(- \dot{\beta} \hat{\delta} - \beta \hat{\delta} + \dot{\beta} \dot{\phi} \cos \delta + \beta \ddot{\phi} \cos \delta - \beta \dot{\phi} \hat{\delta} \sin \delta - \beta \dot{\theta} \sin \delta - \beta \ddot{\theta} \sin \delta - \beta \dot{\theta} \hat{\delta} \cos \delta \right) \\ + \dot{\alpha} \hat{\delta} + \alpha \hat{\delta} + \dot{\alpha} \dot{\phi} \cos \delta + \alpha \ddot{\phi} \cos \delta - \alpha \dot{\phi} \hat{\delta} \sin \delta - \dot{\alpha} \dot{\theta} \sin \delta - \alpha \ddot{\theta} \sin \delta - \alpha \dot{\theta} \hat{\delta} \cos \delta \right) \\ + \dot{\Omega} + \ddot{\theta} \cos \delta - \dot{\theta} \hat{\delta} \sin \delta + \ddot{\phi} \sin \delta + \dot{\phi} \hat{\delta} \cos \delta - \alpha \dot{\phi} \hat{\delta} \sin \delta - \alpha \ddot{\theta} \sin \delta - \alpha \dot{\theta} \hat{\delta} \cos \delta \right) \\ I_{rz} \left(\frac{\sqrt{2}}{2} \left(\hat{\delta} + \ddot{\phi} \cos \delta - \dot{\phi} \hat{\delta} \sin \delta - \ddot{\theta} \sin \delta - \dot{\alpha} \dot{\phi} \sin \delta - \alpha \dot{\phi} \hat{\delta} \cos \delta + \beta \right) \\ - \dot{\alpha} \dot{\theta} \cos \delta - \alpha \ddot{\theta} \cos \delta + \alpha \dot{\theta} \hat{\delta} \sin \delta - \dot{\alpha} \dot{\phi} \sin \delta - \alpha \dot{\phi} \sin \delta - \alpha \dot{\phi} \hat{\delta} \cos \delta + \beta \right) \end{bmatrix}$$
(8)

By substituting Equations (4)–(8) into Equation (1), the rotor torque in rotor frame can be obtained:

$$\mathbf{M}^{\prime} = \begin{bmatrix} -I_{ry}\Omega\left(\frac{\sqrt{2}}{2}\left(\hat{\delta}+\dot{\phi}\cos\delta-\dot{\theta}\sin\delta\right)+\dot{\beta}\right)+\left(I_{rz}-I_{ry}\right)\left(\dot{\theta}\cos\delta+\dot{\phi}\sin\delta\right)\left(\frac{\sqrt{2}}{2}\left(\hat{\delta}+\dot{\phi}\cos\delta-\dot{\theta}\sin\delta\right)+\dot{\beta}\right)\right] \\ +I_{rx}\left(\frac{\sqrt{2}}{2}\left(\hat{\delta}-\ddot{\phi}\cos\delta+\dot{\phi}\hat{\delta}\sin\delta+\ddot{\theta}\sin\delta+\dot{\theta}\hat{\delta}\cos\delta\right)+\dot{\beta}\dot{\theta}\cos\delta+\dot{\beta}\dot{\phi}\sin\delta+\ddot{\alpha}\right) \\ \left(I_{rx}-I_{rz}\right)\left(\frac{\sqrt{2}}{2}\left(\hat{\delta}+\dot{\phi}\cos\delta-\dot{\theta}\sin\delta\right)+\dot{\beta}\right)\left(\frac{\sqrt{2}}{2}\left(\hat{\delta}-\dot{\phi}\cos\delta+\dot{\theta}\sin\delta\right)+\dot{\alpha}\right) \\ +I_{ry}\left(\frac{\sqrt{2}}{2}\left(-\dot{\beta}\hat{\delta}+\dot{\beta}\dot{\phi}\cos\delta-\dot{\beta}\dot{\theta}\sin\delta+\dot{\alpha}\dot{\delta}+\dot{\alpha}\dot{\phi}\cos\delta-\dot{\alpha}\dot{\theta}\sin\delta\right) \\ +\dot{\alpha}+\ddot{\theta}\cos\delta-\dot{\theta}\hat{\delta}\sin\delta+\ddot{\phi}\sin\delta+\dot{\phi}\hat{\delta}\cos\delta-\dot{\alpha}\dot{\theta}+\alpha\ddot{\beta} \\ I_{ry}\Omega\left(\frac{\sqrt{2}}{2}\left(\hat{\delta}-\dot{\phi}\cos\delta+\dot{\theta}\sin\delta\right)+\dot{\alpha}\right)+\left(I_{ry}-I_{rx}\right)\left(\dot{\theta}\cos\delta+\dot{\phi}\sin\delta\right)\left(\frac{\sqrt{2}}{2}\left(\hat{\delta}-\dot{\phi}\cos\delta+\dot{\theta}\sin\delta\right)+\dot{\alpha}\right) \\ +I_{rz}\left(\frac{\sqrt{2}}{2}\left(\hat{\delta}+\ddot{\phi}\cos\delta-\dot{\phi}\hat{\delta}\sin\delta-\ddot{\theta}\sin\delta-\dot{\theta}\hat{\delta}\cos\delta\right)-\dot{\alpha}\dot{\theta}\cos\delta-\dot{\alpha}\dot{\phi}\sin\delta+\ddot{\beta}\right) \end{bmatrix}$$
(9)

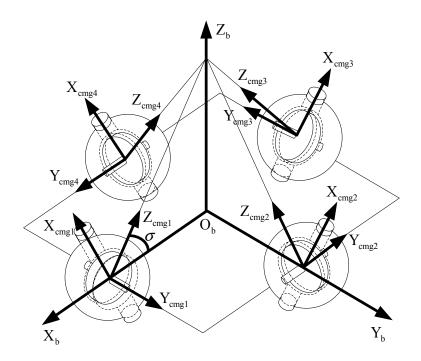
From Equation (9), it can be seen that, for every magnetically suspended SGCMG, $I_{ry}\Omega\hat{\delta}$ is the gyro coupled torque produced by the gimbal rotation relative to the inertial frame. $I_{rr}\hat{\delta}$ is the inertial coupled torque produced by the gimbal. $I_{ry}\Omega\dot{\phi}\cos\delta$ and $I_{ry}\Omega\dot{\theta}\sin\delta$ are the gyro coupled torque produced by the satellite rotation. $I_{rr}\ddot{\phi}\cos\delta$ and $I_{rr}\ddot{\theta}\sin\delta$ are the inertial coupled torque produced by the satellite rotation. $I_{rr}\dot{\phi}\cos\delta$ and $I_{rr}\ddot{\theta}\sin\delta$ are the inertial coupled torque produced by the satellite rotation. $I_{rr}\dot{\alpha}\dot{\alpha}$ are the gyro coupled torque produced by the rotor tilt relative to the magnetic bearing. $I_{rr}\ddot{\alpha}$ and $I_{rr}\ddot{\beta}$ are the inertial coupled torque produced by the rotor accelerating tilt relative to the magnetic bearing.

Equation (9) includes the gimbal angular velocity and the satellite angle acceleration. It shows that there is strong coupling between the rotor, the gimbal and the satellite. Moreover, there are many trigonometric functions, for example, $\sin \delta$ and $\cos \delta$, which shows strongly nonlinear characteristics.

2.2. The Torque of Magnetically Suspended SGCMG Clusters

In this paper, the pyramid configuration using four magnetically suspended SGCMGs is adopted (Figure 4). The frame of the *n*-th CMG can be obtained by rotating the satellite body frame γ_n about the Z_b axis, and then rotating σ_n about the X_b axis. $\gamma = [\gamma_1 \quad \gamma_2 \quad \gamma_3 \quad \gamma_4]^T = [90^\circ \quad 180^\circ \quad 270^\circ \quad 0]^T$, $\sigma = [\sigma_1 \quad \sigma_2 \quad \sigma_3 \quad \sigma_4]^T = [53.13^\circ \quad 53.13^\circ \quad 53.13^\circ \quad 53.13^\circ]^T$.

Figure 4. The pyramid configuration installation of four magnetically suspended SGCMGs.



By rotating the rotor frame 45° in the negative direction of the Y_g axis, rotating $-\delta$ about the X_g axis, and then transforming according to the installation matrix of the pyramid configuration, the attitude transformation matrix \mathbf{C}_r^b from rotor frame to satellite body frame can be obtained. Because the magnetic bearing gap is small, the rotation displacement can be ignored relative to the rotation of the gimbal and the satellite, then $\mathbf{C}_r^f \approx \mathbf{E}$:

$$\mathbf{C}_{r}^{b} = \mathbf{C}_{cmg}^{b} \mathbf{C}_{g}^{cmg} \mathbf{C}_{f}^{g} \mathbf{C}_{r}^{f} \approx \mathbf{C}_{cmg}^{b} \mathbf{C}_{g}^{cmg} \mathbf{C}_{f}^{g}$$
(10)

where

$$\mathbf{C}_{cmg}^{b} = \begin{bmatrix} \sin\sigma\sin\gamma & \cos\gamma & -\cos\sigma\sin\gamma \\ -\sin\sigma\cos\gamma & \sin\gamma & \cos\sigma\cos\gamma \\ \cos\sigma & 0 & \sin\sigma \end{bmatrix}, \\ \mathbf{C}_{g}^{cmg} = \left(\mathbf{C}_{cmg}^{g}\right)^{-1}, \\ \mathbf{C}_{f}^{g} = \begin{bmatrix} \cos45^{\circ} & 0 & \sin45^{\circ} \\ 0 & 1 & 0 \\ -\sin45^{\circ} & 0 & \cos45^{\circ} \end{bmatrix}$$
(11)

The transformation matrix from gimbal frame to body frame is:

$$\mathbf{C}_{g}^{b} = \mathbf{C}_{cmg}^{b} \mathbf{C}_{g}^{cmg} = \begin{bmatrix} \sin\sigma\sin\gamma & \cos\gamma\cos\delta - \cos\sigma\sin\gamma\sin\delta & -\cos\gamma\sin\delta - \cos\sigma\sin\gamma\cos\delta \\ -\sin\sigma\cos\gamma & \sin\gamma\cos\delta + \cos\sigma\cos\gamma\sin\delta & -\sin\gamma\sin\delta - \cos\sigma\cos\gamma\cos\delta \\ \cos\sigma & \sin\sigma\sin\delta & \sin\sigma\cos\delta \end{bmatrix}$$
(12)

Equation (10) can be written as:

$$\mathbf{C}_{r}^{b} = \begin{bmatrix} \frac{\sqrt{2}}{2} \sin \delta \cos \gamma + \frac{\sqrt{2}}{2} \sin \sigma \sin \gamma + \frac{\sqrt{2}}{2} \cos \delta \cos \sigma \sin \gamma & \cos \delta \cos \gamma - \sin \delta \cos \sigma \sin \gamma & -\frac{\sqrt{2}}{2} \sin \delta \cos \gamma + \frac{\sqrt{2}}{2} \sin \sigma \sin \gamma - \frac{\sqrt{2}}{2} \cos \delta \cos \sigma \sin \gamma \\ \frac{\sqrt{2}}{2} \sin \delta \sin \gamma - \frac{\sqrt{2}}{2} \sin \sigma \cos \gamma - \frac{\sqrt{2}}{2} \cos \delta \cos \sigma \cos \gamma & \cos \delta \sin \gamma + \sin \delta \cos \sigma \cos \gamma & -\frac{\sqrt{2}}{2} \sin \delta \sin \gamma - \frac{\sqrt{2}}{2} \sin \sigma \cos \gamma + \frac{\sqrt{2}}{2} \cos \delta \cos \sigma \cos \gamma \\ \frac{\sqrt{2}}{2} \cos \sigma - \frac{\sqrt{2}}{2} \cos \delta \sin \sigma & \sin \delta \sin \sigma & \frac{\sqrt{2}}{2} \cos \sigma + \frac{\sqrt{2}}{2} \cos \delta \sin \sigma \\ \frac{\sqrt{2}}{2} \cos \sigma - \frac{\sqrt{2}}{2} \cos \delta \sin \sigma & \sin \delta \sin \sigma & \frac{\sqrt{2}}{2} \cos \sigma + \frac{\sqrt{2}}{2} \cos \delta \sin \sigma \\ \end{bmatrix}$$
(13)

Then, the absolute angular velocity of the CMG frame can be obtained:

$$\mathbf{C}_{b}^{cmg}\boldsymbol{\omega}_{ib}^{b} + \boldsymbol{\omega}^{g} = \begin{bmatrix} \sin\sigma\sin\gamma & -\sin\sigma\cos\gamma & \cos\sigma\\ \cos\gamma & \sin\gamma & 0\\ -\cos\sigma\sin\gamma & \cos\sigma\cos\gamma & \sin\sigma \end{bmatrix} \begin{bmatrix} \boldsymbol{\omega}_{ibx}^{b}\\ \boldsymbol{\omega}_{iby}^{b}\\ \boldsymbol{\omega}_{ibz}^{b} \end{bmatrix} + \begin{bmatrix} \dot{\delta}\\ 0\\ 0 \end{bmatrix}$$
(14)

The torque generated by the rotor in body frame can be obtained after the sum of four CMGs:

$$\mathbf{M}^{b} = \sum_{n=1}^{4} \mathbf{C}_{r,n}^{b} \mathbf{M}_{n}^{r}$$
(15)

By Equation (15), \mathbf{M}^{b} , the torque of the magnetically suspended SGCMG cluster acting on the three inertial principal axis of the satellite can be obtained.

2.3. Satellite Attitude Dynamic Model Including Magnetically Suspended SGCMGs

The satellite attitude dynamic equation including magnetically suspended SGCMGs can be obtained by the law of angular momentum conservation:

$$\mathbf{J}\dot{\boldsymbol{\omega}}_{ib}^{b} + \boldsymbol{\omega}_{ib}^{b} \times \left(\mathbf{J}\boldsymbol{\omega}_{ib}^{b}\right) + \mathbf{M}^{b} = \mathbf{u}_{d}$$
(16)

where **J** is moment of inertia of the satellite. ω_{ib}^{b} is the angular velocity vector relative to the inertia frame, and it is shown in the body frame. \mathbf{u}_{d} is the environmental disturbance torque, such as aerodynamic drag gravity gradient, solar radiation pressure and Earth magnetic torque. $\omega_{ib}^{b} \times (\mathbf{J}\omega_{ib}^{b})$ represents the gyroscope torque generated by the satellite rotation.

Equation (16) can be simplified to $\mathbf{J}\dot{\mathbf{\omega}}_{ib}^{b} = \mathbf{u}_{c} + \mathbf{u}_{d}$, where \mathbf{u}_{c} is the command control torque acting on the satellite. The command torque for magnetically suspended SGCMGs is:

$$\mathbf{u}_{g} = -\mathbf{u}_{c} - \boldsymbol{\omega}_{ib}^{b} \times \mathbf{H}_{g} - \boldsymbol{\omega}_{ib}^{b} \times \left(\mathbf{J}\boldsymbol{\omega}_{ib}^{b}\right)$$
(17)

where \mathbf{H}_{g} is the total angular momentum of the actuator relative to the satellite body frame. The gimbal angle of four magnetically suspended SGCMGs is $\boldsymbol{\delta} = [\delta_{1} \quad \delta_{2} \quad \delta_{3} \quad \delta_{4}]^{\mathrm{T}}$, where δ_{n} represents the gimbal angle of the *n*-th CMG. By substituting $\boldsymbol{\gamma}$ into Equation (12), the total momentum of four magnetically suspended SGCMGs is:

$$\mathbf{H}_{g} = h_{0} \begin{bmatrix} -\cos\sigma_{1}\sin\delta_{1} - \cos\delta_{2} + \cos\sigma_{3}\sin\delta_{3} + \cos\delta_{4} \\ \cos\sigma_{1} - \cos\sigma_{2}\sin\delta_{2} - \cos\sigma_{3} + \cos\sigma_{4}\sin\delta_{4} \\ \sin\sigma_{1}\sin\delta_{1} + \sin\sigma_{2}\sin\delta_{2} + \sin\sigma_{3}\sin\delta_{3} + \sin\sigma_{4}\sin\delta_{4} \end{bmatrix}$$
(18)

where $h_0 = I_{ry}\Omega$ denotes the rotor angular momentum. Then the variation rate of CMG angular momentum in the satellite body frame can be obtained:

Sensors 2012, 12

$$\mathbf{u}_{g} = \dot{\mathbf{H}}_{g} = \mathbf{C}(\boldsymbol{\delta})\dot{\boldsymbol{\delta}}$$
(19)

where $C(\delta)$ is:

$$\mathbf{C}(\boldsymbol{\delta}) = \begin{bmatrix} -\cos\sigma_{1}\cos\delta_{1} & \sin\delta_{2} & \cos\sigma_{3}\cos\delta_{3} & -\sin\delta_{4} \\ -\sin\sigma_{1} & -\cos\sigma_{2}\cos\delta_{2} & \sin\sigma_{3} & \cos\sigma_{4}\cos\delta_{4} \\ \sin\sigma_{1}\cos\delta_{1} & \sin\sigma_{2}\cos\delta_{2} & \sin\sigma_{3}\cos\delta_{3} & \sin\sigma_{4}\cos\delta_{4} \end{bmatrix}$$
(10)

The command gimbal rate is calculated by the robust pseudo-inverse steering law with null motion [15]:

$$\dot{\boldsymbol{\delta}} = \dot{\boldsymbol{\delta}}_C + \dot{\boldsymbol{\delta}}_N \tag{11}$$

where $\dot{\mathbf{\delta}}_{c}$ denotes the command value calculated by robust pseudo-inverse steering law, $\dot{\mathbf{\delta}}_{N}$ denotes the command value calculated by null motion.

The attitude kinematics are described with the quaternion of the satellite body frame relative to the orbit frame, and then the attitude kinematics equation is:

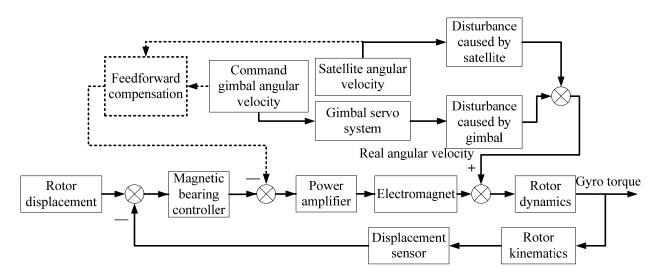
$$\dot{\mathbf{q}} = \frac{1}{2} \mathbf{q} \otimes \boldsymbol{\omega}_{ob} \tag{12}$$

where $\mathbf{q} = [q_0 \quad q_1 \quad q_2 \quad q_3]^T$ represents the attitude quaternion, \otimes means quaternion multiply. The satellite body rate relative to the orbit is $\boldsymbol{\omega}_{ob} = \boldsymbol{\omega}_b - A\boldsymbol{\omega}_o$. *A* is the attitude rotation matrix relative to the orbit frame. $\boldsymbol{\omega}_o = \begin{bmatrix} 0 & -\boldsymbol{\omega}_0 & 0 \end{bmatrix}^T$ is the orbit velocity.

3. Feedforward Compensation for the Rotor Disturbance Torque

When the satellite maneuvers quickly, the satellite angular velocity and gimbal rate will introduce extra torque on the rotor, and the rotor tilt motion will be enhanced. The disturbance torque can be compensated by the feedforward control. Figure 5 gives a diagram of the feedforward compensation.

Figure 5. Sketch of the feedforward compensation.



In order to keep the rotor displacement close to zero, the controller provides the control voltage to maintain the rotor stability. However, the rotation of satellite and gimbal introduces disturbances to the rotor. Feedforward compensation is used to reduce the influence on the rotor. The compensation does not change the control system stability.

The disturbance caused by satellite and gimbal is given in Equation (9). When the satellite body and the gimbal are fixed, $\dot{\delta}$, $\dot{\phi}$ and $\dot{\theta}$ are all zero. The torque is generated by the rotor. Equation (9) is written as:

$$\mathbf{M}^{r}(0) = \begin{bmatrix} -I_{ry}\Omega\dot{\beta} + I_{rx}\ddot{\alpha} \\ (I_{rx} - I_{rz})\dot{\alpha}\dot{\beta} + I_{ry}\left(\dot{\Omega} - \ddot{\alpha}\beta + \alpha\ddot{\beta}\right) \\ I_{ry}\Omega\dot{\alpha} + I_{rz}\ddot{\beta} \end{bmatrix}$$
(13)

Assuming that the rotor acceleration is zero, $\dot{\Omega} = 0$, the rotational inertia of the non-rotation axis is uniform, $I_G = I_O = I_{rr}$, $I_S = I_{rz}$. By ignoring the first order item that includes α and β , the above equation can be simplified as:

$$\mathbf{M}^{r}(0) = \begin{bmatrix} -I_{ry}\Omega\dot{\beta} + I_{rr}\ddot{\alpha}\\ 0\\ I_{ry}\Omega\dot{\alpha} + I_{rr}\ddot{\beta} \end{bmatrix}$$
(14)

By deleting $\mathbf{M}^{r}(0)$ from \mathbf{M}^{r} , the equivalent disturbance torque \mathbf{M}^{r}_{ext} acting on the magnetic bearing control system can be obtained:

$$\mathbf{M}_{ext}^{r} = \begin{bmatrix} -\frac{\sqrt{2}}{2} I_{ry} \Omega \left(\hat{\delta} + \dot{\phi} \cos \delta - \dot{\theta} \sin \delta \right) + \frac{\sqrt{2}}{2} I_{rr} \left(\hat{\delta} - \ddot{\phi} \cos \delta + \dot{\phi} \hat{\delta} \sin \delta + \ddot{\theta} \sin \delta + \dot{\theta} \hat{\delta} \cos \delta \right) \\ 0 \\ \frac{\sqrt{2}}{2} I_{ry} \Omega \left(\hat{\delta} - \dot{\phi} \cos \delta + \dot{\theta} \sin \delta \right) + \frac{\sqrt{2}}{2} I_{rr} \left(\hat{\delta} + \ddot{\phi} \cos \delta - \dot{\phi} \hat{\delta} \sin \delta - \ddot{\theta} \sin \delta - \dot{\theta} \hat{\delta} \cos \delta \right) \end{bmatrix}$$
(15)

Since $I_{rz}\Omega >> I_{rr}$, the gimbal and satellite have more influence on the rotor than their angle acceleration. It is to say, the gyro coupling torque is more obvious than the inertia coupling torque. In designing the steering law, the limited gimbal angular velocity must be considered to prevent the instability. The gimbal angle acceleration should be limited to improve the dynamic response ability.

4. Simulation Results and Analysis

The initial satellite attitude angle is $[-20^{\circ} \ 50^{\circ} \ 30^{\circ}]^{T}$. The target satellite attitude angle is $[0^{\circ} \ 0^{\circ} \ 0^{\circ}]^{T}$. The moment of inertia of the satellite is $[12 \ 12 \ 6]^{T} \text{kg} \cdot \text{m}^{2}$. The initial gimbal angle is $[90^{\circ} \ -90^{\circ} \ 90^{\circ} \ -90^{\circ}]^{T}$. The radial inertia of the magnetically suspended rotor is $I_{rx} = I_{ry} = I_{rr} = 0.0034 \text{kg} \cdot \text{m}^{2}$, the axial inertia is $I_{rz} = 0.0052 \text{kg} \cdot \text{m}^{2}$, the speed of the rotor is 15,000 r/min. $\Omega = 500\pi \text{rad/s}$.

4.1. The Comparison of with and without Feedforward Compensation not Using an Attitude Control Loop

In this section, aiming at the dynamic characteristics of a single gimbal magnetically suspended CMG, the simulation is performed without the attitude control loop. The gimbal acceleration is $120^{\circ}/s^2$, the maximal gimbal rate is $10^{\circ}/s$, and the simulation period is 3 s. The gimbal rate limit is $\delta_{max} = 10^{\circ}/s$. Figures 6 and 7 are the simulation results of with and without feedforward compensation. From the local zoom in of Figures 6(a) and 7(a), it can been seen that, the vibration displacement range is decreased to some degree after using the feedforward compensation, and then a faster response and the higher precision of the output torque can be obtained. From the comparison of Figure 6(b) with Figure 7(b), it can be seen that the overshooting of control current is reduced by using feedforward compensation, and the power consumption is decreased. Because the magnetic bearing control frequency is highly relative to the satellite motion, the disturbance torque induced from the satellite angle velocity can be compensated by the feedforward loop.

Figure 6. The curves without feedforward compensation. (a) Magnetic bearing torque; (b) Control current; (c) The rotor tilt angle; (d) The rotor tilt angle velocity; (e) The rotor displacement of A-side; (f) The rotor displacement of B-side.

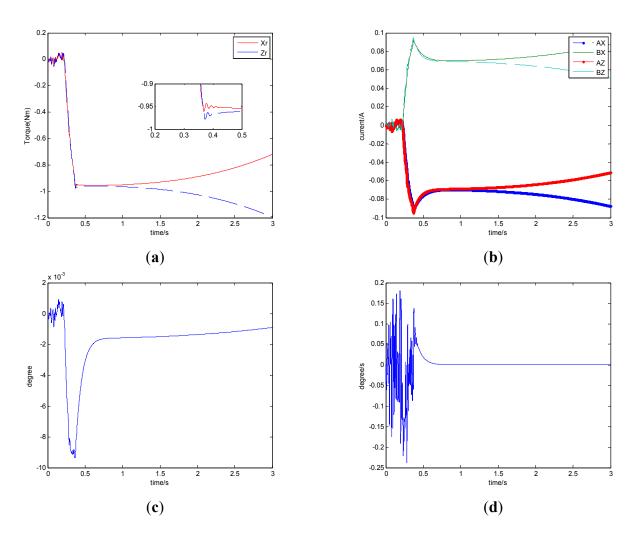


Figure 6. Cont.

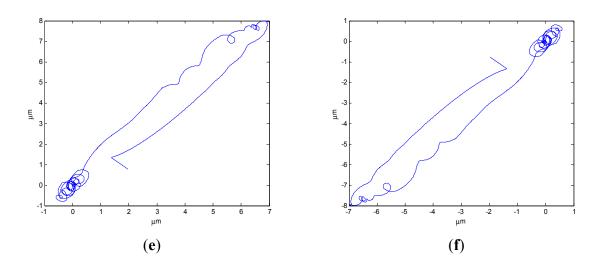


Figure 7. The curves with feedforward compensation. (a) Magnetic bearing torque; (b) Control current; (c) The rotor tilt angle (d) The rotor tilt angle velocity; (e) The rotor displacement of A-side (f) The rotor displacement of B-side; (e) The rotor displacement of A-side; (f) The rotor displacement of B-side.

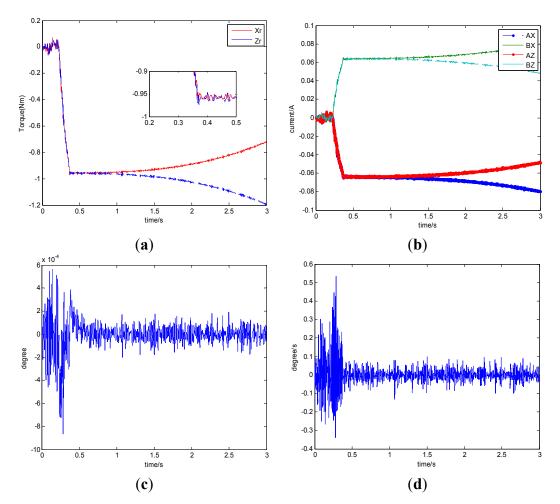
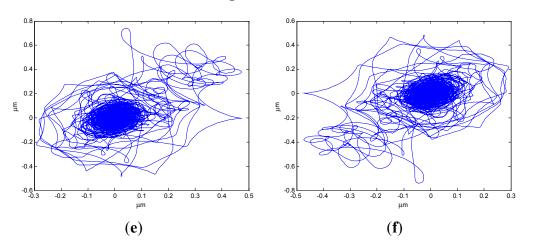


Figure 7. Cont.



Figures 6(c) and 7(c) give the extent of tilt of the rotor relative to the magnetic bearing. It can be seen that after using feedforward compensation, the tilt extent is reduced, but the relative tilt angle velocity is increased, which can be seen from Figures 6(d) and 7(d). Figures 6(e,f) and 7(e,f) correspond to the displacement of the two sides of the rotor. It can be seen that the rotor displacement in the maneuvering process is reduced apparently by the feedforward compensation.

4.2. The Comparison of with and without Feedforward Compensation Using Attitude Control Loop

The attitude control period is 0.5 s. The maximal gimbal rate is $\dot{\delta}_{max} = 10^{\circ}/s$. The simulation results of the three-axis attitude control of the satellite with feedforward compensation are given in Figures 8–13. Figure 8 is the satellite attitude angle. Figure 9 is the satellite angle velocity. Figure 10 gives the gimbal rates of four magnetically suspended SGCMGs. Figure 11 gives the gimbal angles of four magnetically suspended SGCMGs. Figure 12 is the satellite angle acceleration.

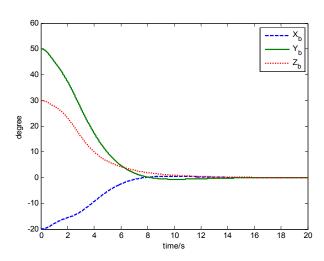


Figure 8. Satellite attitude angle.

Figure 9. Satellite angle velocity.

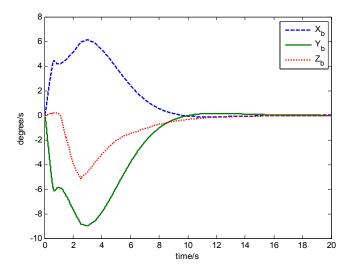


Figure 10. The gimbal rates of magnetically suspended SGCMGs.

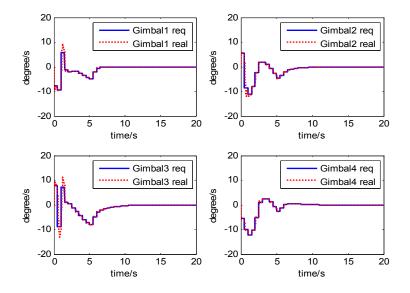
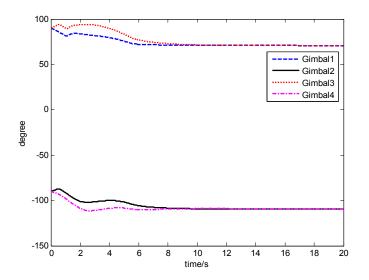


Figure 11. The gimbal angle of magnetically suspended SGCMGs.



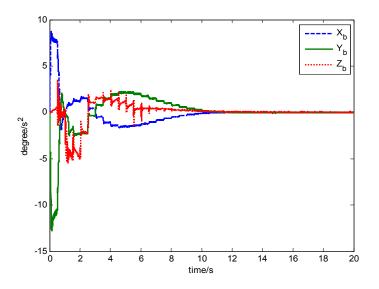
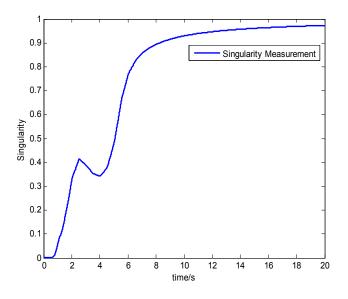


Figure 12. Satellite angle acceleration.

Figure 13. Singularity measurement curves.



The magnetic bearing force in each channel depends on the magnetic bearing coefficient, the magnetic gap of the two sides of the magnetic bearing, the bias current, the rotor displacement and the control current, *etc.* When the magnetic bearing design is finished, it is determined by the magnetic bearing coefficient and magnetic bearing gap. By adjusting the control current, the magnetic bearing force is changed to assure the convergence of rotor displacement, but the magnetic bearing force has a nonlinear relationship with the rotor displacement and the control current. The magnetic bearing controller is used to make sure the stability under the working point.

In Figures 14–19, the left column gives the rotor X-Y displacement, the magnitude of rotor displacement and control current without feedforward compensation. The right column gives the results with feedforward compensation.

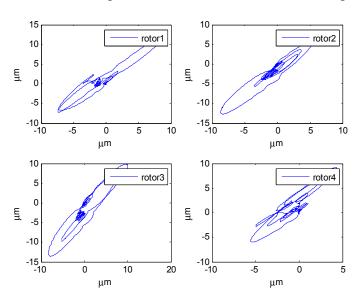


Figure 14. The rotor displacement without feedforward compensation.

Figure 15. The rotor displacement with feedforward compensation.

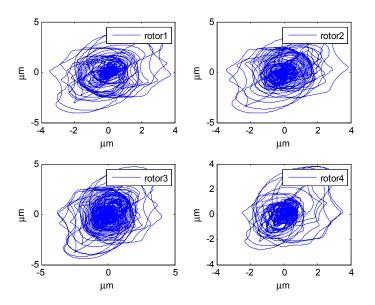
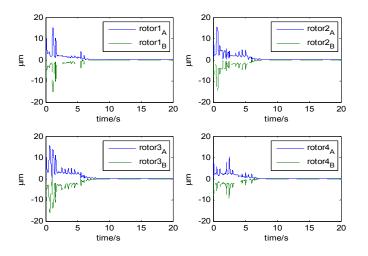


Figure 16. The magnitude of the rotor displacement without feedforward compensation.



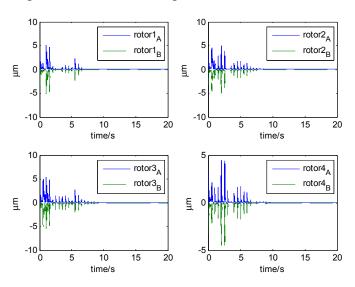
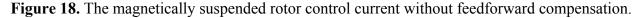


Figure 17. The magnitude of the rotor displacement with feedforward compensation.



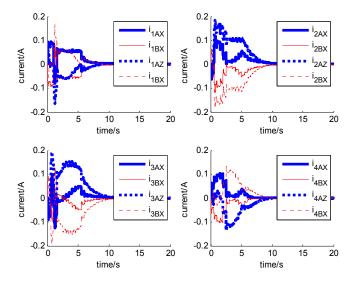
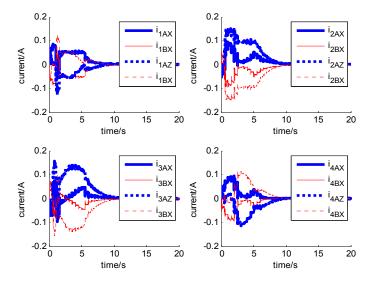


Figure 19. The magnetically suspended rotor control current with feedforward compensation.



It can be seen that, after using feedforward compensation, the rotor displacement is reduced to about 30%, which decreases the risk of the rotor instability. Figures 18–19 show that the control current does not vary apparently. Although the rotor displacement and the given control current are reduced, extra control current is needed for feedforward compensation. It is to say, the command torque is invariant. The torque is output by the control current to assure the stable suspending of the rotor, and so the control current did not vary apparently. By using feedforward compensation, the maximal displacement of the rotor is less than 10% of the magnetic bearing protecting gap, which can ensure the requirement of the stability of magnetically suspended rotor. Figures 20–23 give α , β , $\dot{\alpha}$ and $\dot{\beta}$ of the magnetically suspended SGCMG rotor, which describe the motion of the rotor relative to the magnetic bearing.

Figure 20. The magnetically suspended rotor tilt curves relative to rotor center before compensation.

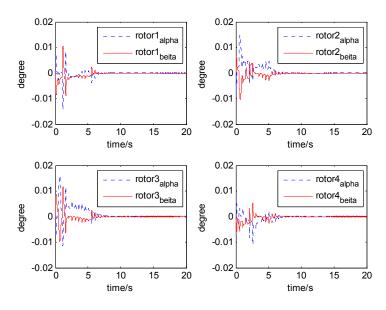
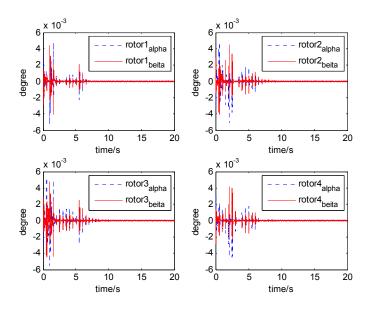


Figure 21. The magnetically suspended rotor tilt curves relative to rotor center after compensation.



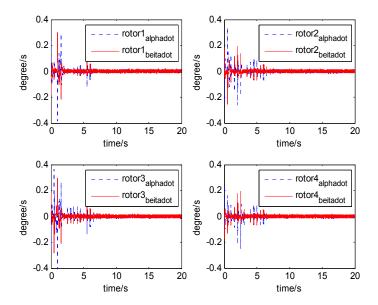
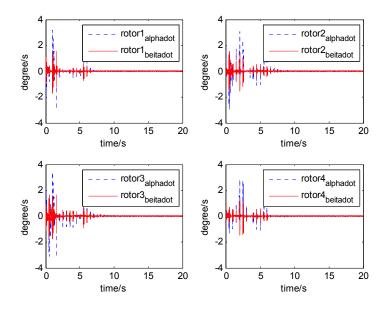


Figure 22. The magnetically suspended rotor angle velocity relative to rotor center before compensation.

Figure 23. The magnetically suspended rotor angle velocity relative to rotor center after compensation.



By using feedforward compensation for the magnetically suspended control system, the response of angle acceleration and angle velocity becomes faster owing to the increase of the control current, which decreases the rotor angle displacement. There is a magnetic saturation problem in the magnetic bearing design, so there exists a magnetic bearing control current saturation limit. When the satellite and the gimbal rate exceed the limit, the additional disturbance torque on the rotor is large, which exceeds the extent of the control current, and then the rotor becomes instable, even resulting in CMG failure. This will influence the stability of the whole system. When the maximal gimbal rate limit is $\dot{\delta}_{max} = 12^{\circ}/s$, the results of not using feedforward compensation are shown in Figures 24 and 25.

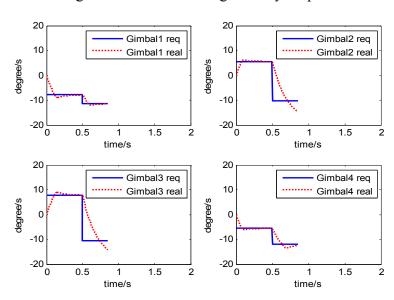
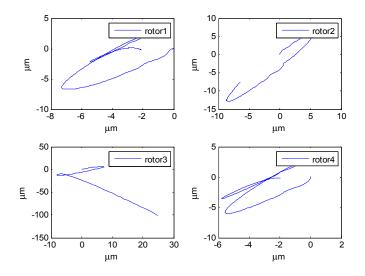


Figure 24. The gimbal rate of four magnetically suspended SGCMGs.

Figure 25. The rotor X-Y displacement without feedforward compensation.



The terminative condition of the simulation is whether the rotor displacement exceeds the magnetic gap (100 μ m) or not. The above figures show that, the simulation finish in less than 1 s. The reason is that magnetically suspended SGCMG3 becomes instable. Because the gimbal angular acceleration command limit is not performed, the overshooting of gimbal servo system results in the real gimbal rate being larger than 12°/s, and then the equivalent additive magnetic bearing torque is large, which results in an increase of the rotor displacement. There exists the magnetic bearing control current saturation limit, it is difficult to provide sufficient magnetic bearing torque, which results in the rotor displacement exceeding the approximately linear zone and reaching the magnetic gap instantaneously, and then the magnetically suspended rotor becomes instable. In the end, the stability of magnetic bearing control system and satellite control system are destroyed.

The curves of gimbal rate and rotor displacement with feedforward compensation are given in Figures 26 and 27.

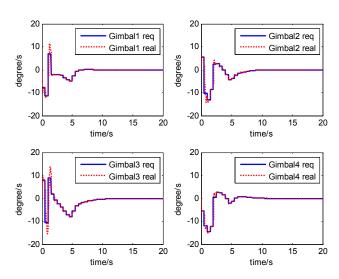
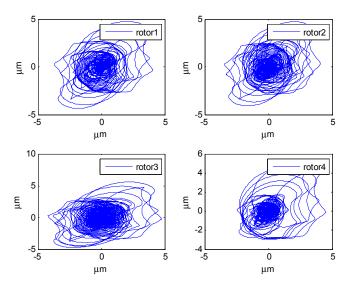


Figure 26. The gimbal rate of four magnetically suspended SGCMGs with feedforward compensation.

Figure 27. The rotor displacement with feedforward compensation.

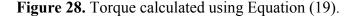


It can be seen that the rotor displacement is reduced by the feedforward compensation. Although there is overshooting of the gimbal rate, even exceeding 14° /s, the displacement of the rotor is less than 5 µm. This ensures the normal use of the magnetically suspended SGCMG. There are also some research results that are related to the compensation and disturbance attenuation [16–19]. In the future, the advanced algorithm will be employed.

4.3. Analysis on the Output Torque

The output torque of magnetically suspended SGCMG includes the inertial coupled torque and the gyro coupled torque, which is produced from the coupling of the satellite, the gimbal and the rotor. Traditionally, the inertial coupled torque is ignored when Equation (19) is used to calculate the output torque according to the Jacobian matrix and the gimbal rate. In this paper, the total torque is produced from the magnetically suspended rotor dynamic equation, as shown in Equation (15). By using this method, a more actual output torque of the actuator can be obtained. This is important for the analysis

of the agile satellite attitude control system. Equation (15) also includes the strong coupling relationship between the rotor, gimbal, and satellite. This results in strongly nonlinear in the trigonometric function item that is relative with the gimbal angle. Figure 28 shows the torque calculated from Equation (19). Figure 29 gives the total output torque calculated from Equation (15).



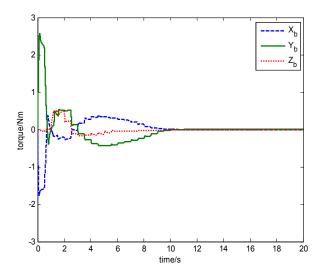
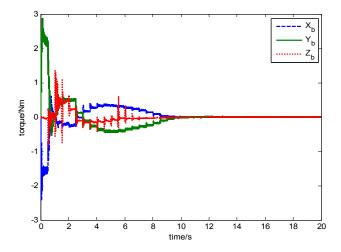


Figure 29. Torque calculated using Equation (15).



From the simulation results, it can be seen that the trend of torque curves calculated using Equations (15) and (19) are consistent. Figure 29 shows the influence of the rotor imbalance vibration and gimbal system, which is high frequency compared with the satellite attitude control system, so in the simulation, the torque model in Equation (15) should be used, which can emulate the dynamic characteristics of a magnetically suspended SGCMG more really. In the feedforward compensation for a magnetically suspended rotor, the compensation should be performed according to the rotation rate of the CMG frame with respect to the inertial frame, so in a situation of satellite rapid maneuver, the dynamic modeling of the magnetically suspended SGCMG is very important. The simulation results show that it coincides with the theoretical analysis results.

5. Conclusions

With magnetically suspended SGCMGs mounted as a pyramid, the modeling of satellite attitude dynamic is built, and feedforward compensation control is used. The simulation results are given to show that by using the feedforward control, the displacement of the rotor is reduced. This is important for the future semi-physics experiment, and becomes the basis for the application of a single gimbal magnetically suspended CMG in agile satellites.

Acknowledgements

This research has been supported by National Natural Science Foundation of China under Grant No. 61121003, the National Basic Research Program (973 Program) of China under Grant No. 2009CB72400101C and National Civil Aerospace Pre-research Project.

References

- 1. Wie, B.; Heiberg, C.; Bailey, D. Rapid Multi-Target Acquisition and Pointing Control of Agile Spacecraft. J. Guid. Contr. Dyn. 2002, 25, 96–104.
- 2. Lappas, V.; Steyn, W.H.; Underwood, C. Design and Testing of a Control Moment Gyroscope Cluster for Small Satellites. *J. Spacecraft Rockets* **2005**, *42*, 729–739.
- Toizumi, T.; Enomoto, T.; Yatsu, Y.; Nakamori, T.; Kawai, N.; Ishizaka, K.; Muta, A.; Morishita, H.; Akiyama, K.; Kisa, N.; *et al.* Development of the Small Satellite "Tsubame". *Phys. E Low Dimens. Syst. Nanostruct.* 2011, 43, 685–688.
- 4. Wei, T.; Fang, J.C. Moving-Gimbal Effects and Angular Rate Feedforward Control in Magnetically Suspended Rotor System of CMG (in Chinese). J. Astron. 2005, 26, 19–23.
- Liu, H.; Li, J.F. SGCMG Steering Law Design for Agility Spacecraft Reorientation (in Chinese). J. Astron. 2006, 27, 113–116.
- Ahrens, M.; KuEera, L. Cross Feedback Control of a Magnetic Bearing System. In *Proceedings of* the 3rd International Symposium on Magnetic Suspension Technology, Tallahassee, FL, USA, 13–15 December 1995; pp. 13–15.
- Wei, T.; Fang, J.C.; Liu, Z.R. Moving-Gimbal Effects Compensation of Double Gimbal Magnetically Suspended Control Moment Gyroscope Based on Compound Control (in Chinese). *J. Mech. Eng.* 2010, 46, 159–165.
- 8. Kwon, S. Attitude Control of Small Satellites Using Single-Gimbal Control Torque Gyros. Ph.D. Thesis, Osaka Prefecture University, Osaka, Japan, 2010.
- 9. Wie, B. New Singularity Escape/Avoidance Steering Logic for Control Torque Gyro Systems. In *Proceedings of AIAA Guidance, Navigation, and Control Conference and Exhibit*, Austin, TX, USA, 11–14 August 2003.
- Lappas, V.J.; Oosthuizen, P.; Madle, P. Design, Analysis and In-Orbit Performance of the BILSAT-1 Microsatellite Twin Control Moment Gyroscope Experimental Cluster. In *Proceedings* of AIAA Guidance, Navigation, and Control Conference and Exhibit, Providence, RI, USA, 16–19 August 2004.

- 11. Kwon, S.; Shimomuraa, T.; Okuboa, H. Pointing Control of Spacecraft using Two SGCMGs via LPV Control Theory. *Acta Astron.* **2011**, *68*, 1168–1175.
- 12. Heiberg, C.J. A Practical Approach to Modeling Single-Gimbal Control Moment Gyroscope in Agile Spacecraft. In *Proceedings of AIAA Guidance, Navigation, and Control Conference and Exhibit*, Denver, CO, USA, 14–17 August 2000.
- 13. Yang, B.H. *Guidance, Navigation and Control of Aircraft*; China Science and Technology Press: Beijing, China, 2011.
- 14. Duan, H.D.; Wu, Z. Dynamics and Simulation of Spacecraft with Magnetically Suspended Control Moment Gyroscope (in Chinese). J. Syst. Simulat. 2009, 21, 2783–2786.
- Tao, M.; Saburo, M. Modified Singular-Direction Avoidance Steering for Control Moment Gyros. J. Guid. Contr. Dyn. 2011, 34, 1915–1919.
- Zhang, H.; Shi, Y.; Saadat Mehr, A. Robust H∞ PID Control for Multivariable Networked Control Systems with Disturbance/Noise Attenuation. *Int. J. Robust Nonlin. Contr.* 2009, 22, 183–204.
- 17. Zhang, H.; Shi, Y.; Saadat Mehr, A. Robust Static Output Feedback Control and Remote PID Design for Networked Motor Systems. *IEEE Trans. Ind. Electron.* **2011**, *58*, 5396–5405.
- Yu, B.; Shi, Y.; Huang, J. Modified Generalized Predictive Control of Networked Systems with Application to a Hydraulic Position Control System. *ASME J. Dynam. Syst. Measur. Contr.* 2011, 133, 031009.
- 19. Shi, Y.; Yu, B. Robust Mixed h₂/h_∞ Control of Networked Control Systems with Random Time Delays in Both Forward and Backward Communication Links. *Automatica* **2011**, *47*, 754–760.

© 2012 by the authors; licensee MDPI, Basel, Switzerland. This article is an open access article distributed under the terms and conditions of the Creative Commons Attribution license (http://creativecommons.org/licenses/by/3.0/).